Journal of Catalysis **200,** 330–339 (2001)
doi:10.1006/jcat.2001.3212, available online at http://www.idealibrary.com on IDEAL®

Structure–Reactivity Relationships on Supported Metal Model Catalysts: Adsorption and Reaction of Ethene and Hydrogen on $Pd/Al_2O_3/NiAl(110)$

Sh. Shaikhutdinov,*,[1] M. Heemeier,* M. Bäumer,* T. Lear,† D. Lennon,† R. J. Oldman,‡ S. D. Jackson,§ and H.-J. Freund*

*Fritz-Haber-Institut der Max-Planck-Gesellschaft, Berlin 14195, Germany; †Department of Chemistry, University Glasgow, Glasgow G12 8QQ, U.K.; ‡ICI Technology, P.O. 8, The Heath Runcorn,Cheshire WA7 4QD,U.K.; and §ICI Synetix, P.O. 1, Billingham, Cleveland TS23 1LB, U.K.

Received November 19, 2000; revised February 10, 2001; accepted February 10, 2001; published online May 15, 2001

Adsorption and co-adsorption of ethene (C_2H_4, C_2D_4) and hydrogen (D_2) on Pd particles deposited on a thin alumina film were studied by temperature-programmed desorption (TPD). The morphology and Pd particle size were controlled by the deposition parameters and monitored by scanning tunneling microscopy. The TPD spectra change gradually as a function of particle size. The size effect for ethene adsorption is attributed to a redistribution between weakly bound π- and more strongly bound di-σ-ethene, with the di-σ-ethene molecule preferentially adsorbed on the larger particles. Deuterium adsorption results in D atoms located on the surface and, in addition, presumably in subsurface sites. Hydrogen atoms adsorb more strongly on the surface of smaller particles, while binding in subsurface sites is less strong and only weakly dependent on particle size. Hydrogen pre-adsorption shifts the distribution of ethene states toward the weakly bound π-state, while adsorbed ethene blocks the hydrogen adsorption. Upon co-adsorption, ethane is produced by the reaction of the π-bonded ethene with those hydrogen atoms residing in the most weakly bound sites. The ethene hydrogenation activity of Pd is independent of the particle size in the 1–3 nm range under the conditions studied. We rationalize this on the basis of the above observations.

Key Words: **ethene; hydrogen; palladium; adsorption; hydrogenation; temperature–programmed desorption; scanning tunneling microscopy; size effect.**

INTRODUCTION

A determination of the relationship between the structure and the properties of small metal particles and clusters is of fundamental importance for many technical applications, particularly in catalysis and materials science.

A number of reviews have recently been published discussing the different approaches to understanding mechanisms of catalytic reactions at a molecular level (1–6). For these purposes, the preparation of well-defined systems which model highly dispersed metals supported on oxides is essential. A systematic investigation of structure–reactivity correlations in such systems is then possible since the system parameters can be varied in a controllable way. In this context, metal particles deposited onto thin oxide films have been found to represent suitable model systems (6, 7). When thin oxide films on metallic substrates are used instead of oxide bulk materials, many powerful surface sensitive techniques, such as various electron spectroscopies and scanning tunneling microscopy, can be applied for the characterization of the metal/oxide surface without facing "charging" problems (3, 5).

In the past few years, we have extensively studied a number of metals vapor-deposited on a thin, well-ordered alumina film grown on a NiAl(110) single crystal. It has been found that most transition metals form three-dimensional aggregates with a relatively narrow particle size distribution (5–7). By controlling the deposition parameters, i.e., substrate temperature and vapor flux, the morphology and size of the metal particles can be reproducibly varied. In principle, this allows determination of the relationship between the structure and reactivity of oxide-supported metal particles. Inspired by this idea, we have carried out a detailed study of the adsorption properties of the model systems using CO as a probe molecule and have recently extended this work to adsorption of ethene, as one of the simplest hydrocarbons, aimed at the investigation of olefin hydrogenation reactions (7).

Palladium is known as a good catalyst for hydrocarbon hydrogenation reactions. To date, such reactions are considered to be structure insensitive (8). However, it has been shown that, for instance, butene hydrogenation on highly dispersed Pd/Al_2O_3 catalysts exhibits a particle size effect: the larger the particle, the lower the turnover number (9). In addition, very small Pt particles have been found to be more active for the hydrogenation of ethene (10) and propene(11).

Adsorption of ethene on Pd has been the subject of extensive studies on single-crystal surfaces and supported catalysts [see reviews by Sheppard and De La Cruz (12, 13)]. At low temperatures, ethene may adsorb on Pd surfaces either in a π-bonding configuration with a near sp^2

[1] To whom correspondence should be addressed. Fax: ++49-30-8413-4101. E-mail: shaikhutdinov@fhi-berlin.mpg.de.

0021-9517/01 $35.00

hybridization of the carbon atoms or in a di-σ-bonding geometry with a near sp^3 hybridization. Upon heating, ethene dehydrogenates and can form several surface species, depending on metal surface symmetry, temperature, and coverage. Formation of ethylidyne ($\equiv C-CH_3$), ethynyl ($-C\equiv CH$), and vinyl ($=CH-CH_2$) species as stable intermediates of ethene thermal transformations has been suggested on the Pd(111), Pd(110), and Pd(100) surfaces, respectively (14–16). On finely dispersed Pd particles, vibrational spectroscopy data clearly indicate that ethene preferentially adsorbs in a π-bonded geometry at 90 K. However, it is the di-σ- rather than the π-complex that transforms into ethylidyne upon warming to room temperature (12). At elevated temperatures (ca. 500–600 K), only a carbon overlayer remains on the surface due to complete ethene decomposition.

Concerning the interaction of hydrogen with palladium, it is well documented that hydrogen readily dissociates on Pd. Subsequently, hydrogen atoms can migrate into the bulk and/or subsurface layers. The system behavior (adsorption, absorption, Pd hydride formation) depends on many parameters such as reaction temperature, gas pressure, and Pd crystallite size (17, 18). For the case of low hydrogen pressures typically used in "surface science" studies, the mechanism of the H_2/Pd reaction is still debated even for well-defined Pd single-crystal surfaces, particularly concerning the nature of the subsurface hydrogen [see reviews of Christmann (17, 19, 20)]. Obviously, these issues are much more complicated in the case of small Pd aggregates.

In the present paper, we have performed a temperature-programmed desorption (TPD) study of ethene and hydrogen adsorption on the Pd particles in order to investigate the structure–reactivity relationships in olefin hydrogenation reactions on Pd. The structure of the Pd/Al_2O_3/NiAl(110) system was monitored by scanning tunneling microscopy (STM). The adsorption and co-adsorption of ethene and hydrogen have been investigated by TPD of regular and isotope-labeled ethene (C_2H_4, C_2D_4) and deuterium (D_2).

EXPERIMENTAL

The experiments were performed in two separate ultra-high-vacuum (UHV) chambers. The first was equipped with STM, low-energy electron diffraction (LEED), and Auger electron spectroscopy (AES) (all from Omicron) and X-ray photoelectron spectroscopy (XPS) (Leybold Hereaus), the second vacuum chamber ("TPD chamber") with LEED/AES, and a quadrupole mass spectrometer (QMS) (Fisons) for TPD measurements. The base pressure in both chambers was below 10^{-10} mbar. In order to compare the data obtained in the two UHV systems, an identical sample preparation recipe was used (21). This involved the preparation of the thin alumina film by oxidation of the clean NiAl(110) surface in 10^{-6} mbar of oxygen at 550 K for 20 min followed by an annealing step in vacuum at 1140 K for 5 min. Palladium (99.99%, Goodfellow) was deposited onto the alumina film using an electron beam-assisted evaporator (Omicron). Typical deposition rates were about 0.6 Å min^{-1}, as calibrated with a quartz microbalance.

In the TPD chamber, a NiAl(110) single crystal of $8 \times 10 \times 1$ mm^3 was spot-welded to two parallel Ta wires for resistive heating. The temperature was measured by a chromel–alumel thermocouple spot-welded to the back side of the crystal. Cooling to about 80 K was achieved by filling a manipulator rod with liquid nitrogen.

The adsorption was performed with a directional gas doser in order to minimize contamination of the vacuum chamber. The doser was calibrated by comparing TPD spectra of CO on the clean NiAl(110) surface with spectra obtained by back-filling the chamber. Oxygen (99.999%), argon (99.999%), ethene (C_2H_4, 99.95%), and deuterium (99.9%, isotopic content 99.5%) were supplied by AGA Gas GmbH, and C_2D_4 (isotope content 99%) by Isotec Inc. A few experiments were performed by adsorption of C_2D_4 purified by bulb-to-bulb distillation.The TPD spectra, however, were found to be nearly identical to those obtained without purification.

The mass spectrometer had a differentially pumped shield with an aperture of 6 mm. For the TPD measurements, the nozzle of the shield was placed about 0.5 mm in front of the sample surface to minimize the signal coming from the sample heating wires. A linear temperature ramp to 550 K with a heating rate of 5 K s^{-1} was generated using a feedback control system (Schlichting Phys. Instrum.). The computer-multiplexed mass spectrometer allowed up to 16 masses to be simultaneously monitored. The spectra presented here were not corrected for ionization gauge sensitivities.

The TPD experiments were performed as follows. First, palladium was deposited on an alumina film kept at 90 K. After deposition, the sample was flashed to ~400 K and cooled to 90 K for ethene adsorption or to 195 K for deuterium adsorption. Since ethene irreversibly adsorbs on Pd producing carbonaceous deposits at elevated temperatures, it was necessary to prepare new samples after each TPD run.

STM images were obtained at room temperature at tunneling voltages of 3.5–4 V applied to the sample and a current of 0.5–1 nA. The images were subjected to plane subtraction.

RESULTS AND DISCUSSION

Morphology of the Pd/Alumina Surface

The STM images presented in Fig. 1 show characteristic morphologies of the Pd/Al_2O_3/NiAl(110) surface. The

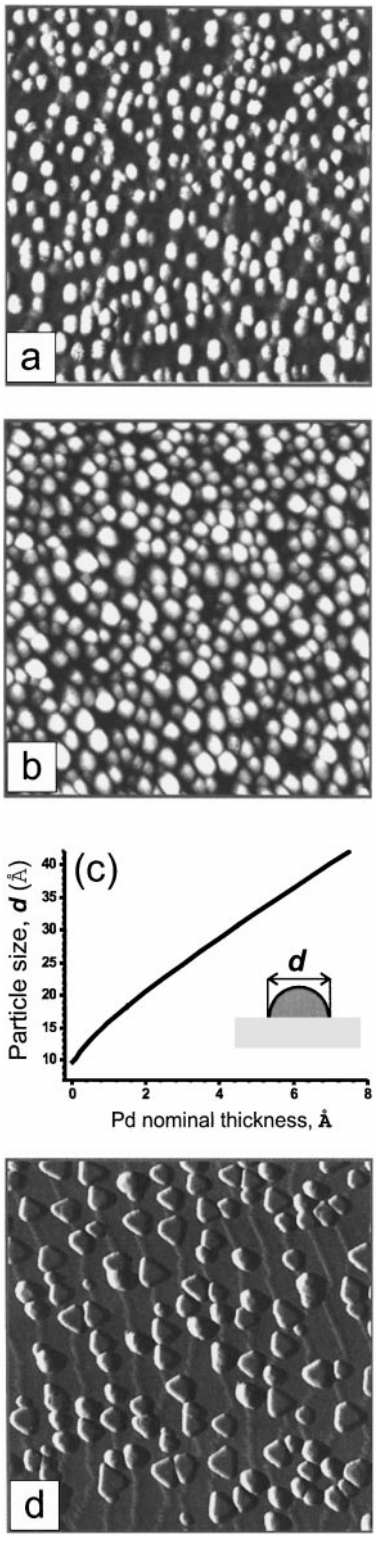

FIG. 1. Room temperature STM images (size 1000 × 1000 Å^2) of Pd aggregates grown on Al_2O_3/NiAl(110) by deposition at 90 K (a, b) and 300 K (d). In the latter case, the image is presented with differentiated contrast to show the network of domain boundaries. The nominal Pd thickness is 0.2 Å (a) and 2 Å (b, d). (c) The size of Pd particles deposited at 90 K as a function of the Pd nominal thickness assuming a hemispherical particle shape.

surface structure critically depends on the deposition temperature. When deposited at 90 K, the particles are uniformly distributed on the support, as shown in images (a) and (b), due to preferential nucleation at point defects existing on the film (22). At room temperature, the particles mostly nucleate at line defects (domain boundaries and steps) of the alumina substrate as shown in image (d). In the latter case, the particles are well-defined and expose mainly (111) facets, as has been recently demonstrated by atomically resolved STM images (23).

STM images have revealed that the particle size increases gradually with the amount of Pd deposited, in agreement with a spot-profile analysis LEED study (6). However, the lateral dimension of the metal aggregates determined directly from STM is usually overestimated by a factor of 2, due to tip convolution effects (24). Instead, it is more adequate to use the average number of atoms per particle as an indicator of the particle size. This number can be calculated from the island density and the Pd nominal thickness, as measured by STM and a quartz microbalance, respectively. We have recalculated the average number of atoms into a "mean particle size" assuming a hemispherical shape for the metal aggregates. The corresponding relationship between Pd nominal thickness and particle diameter for the case of deposition at 90 K is shown in Fig. 1c. By controlling the deposition flux and the substrate temperature, a high reproducibility for the particle size has been achieved.

STM inspection of the Pd/alumina surface after a TPD run to 550 K revealed that the particle density remained the same. However, the local arrangement of the surface Pd atoms is influenced by warming to room temperature, as previously demonstrated by infrared reflection adsorption spectroscopy (IRAS) (7, 25). In the present paper, this has been corroborated by comparing TPD spectra of ethene from samples prepared at 90 K with those obtained on the identical samples after annealing to 400 K (see below). Probably, the particles reach a more regular shape at elevated temperatures due to the increasing mobility of the Pd surface atoms. In order to minimize the influence of such effects on the TPD spectra, we briefly heated ("flashed") all samples to 400 K prior to the TPD experiments. In addition, this procedure results in desorption of hydrogen that adsorbs on Pd during metal deposition at 90 K, even at a background pressure below 3×10^{-10} mbar.

Ethene Adsorption

Ethene adsorption on the clean alumina film at 80 K does not result in any significant TPD signals. Therefore, we conclude that ethene does not adsorb on the pristine alumina film at and above 80 K, in agreement with previous results (26). In the TPD spectra recorded after C_2H_4 adsorption on the Pd samples, C_2H_4, H_2, and negligible amounts of CO are detected as the only desorbing products. [In the following, we use the 27 amu signal corresponding to ethene

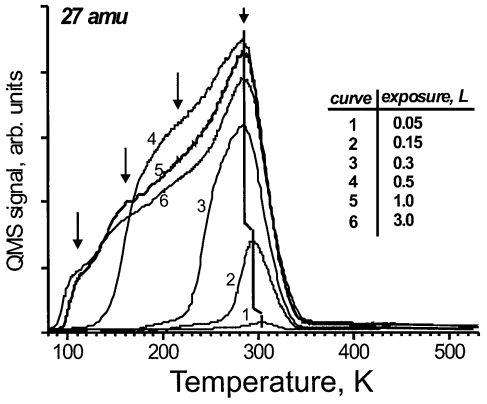

FIG. 2. TPD spectra of ethene (C_2H_4) obtained for identically prepared samples (the mean Pd particle size is about 20 Å) after various exposures of ethene at 90 K. Several desorption states are observed at saturation and marked by the arrows.

fragmentation ($C_2H_3^+$) in order to discriminate ethene and CO].

Figure 2 shows a family of TPD spectra of ethene obtained for different exposures on identically prepared Pd particles about 20 Å in diameter. The integral TPD signal increases with exposure and reaches saturation at about 1 L (1 L $= 10^{-6}$ Torr s). At subsaturation exposures, the intensity of the peak near room temperature increases and shifts by ~20 K to lower temperatures with increasing exposure. At saturation exposure, ethene desorbs in a broad signal between 90 and 350 K, exhibiting a number of desorption states as indicated by the arrows. The states are sequentially filled with increasing exposure. No ethene multilayer is formed, in line with a previous IRAS study (7, 27).

Figure 3a shows TPD spectra of ethene obtained after adsorption of 1 L of C_2H_4 on Pd particles of different size. As the particle size increases, the TPD spectra change gradually, with the peak near room temperature becoming dominant in the spectra. This trend is clearly seen in the normalized representation shown in Fig. 3b. For the largest Pd particles studied (>30 Å), the TPD spectrum is similar to those observed for the Pd single-crystal surfaces with a dominant desorption peak at around 300 K (16, 28, 29).

TPD spectra of H_2 (2 amu) simultaneously recorded with ethene are presented in Fig. 3c. The plateau-like signal at temperatures below 270 K results from ethene cracking in the mass spectrometer and can be properly subtracted. The peak at ~330 K, denoted as β_2, shifts by about 15 K to lower temperatures as the particle size increases. Two desorption peaks (γ), centered at ca. 400 and 450 K, emerge for the largest particles.

The TPD spectra recorded for deuterium-substituted ethene, C_2D_4, exhibit a similar behavior (see, for instance, Fig. 7a). Therefore, hydrogen developed during a TPD run obviously originates from ethene dehydrogenation on heating. We should mention, however, the additional uptake of hydrogen from the vacuum background during cooling of the sample before ethene adsorption, that results in higher relative intensity of the H_2 (D_2) β_2 peak with respect to the γ peak in the case of C_2H_4 adsorption as compared to C_2D_4.

The β_2 peak is attributed to the primary ethene dehydrogenation steps, while the γ peaks can be assigned to the further stepwise decomposition of the dehydrogenated hydrocarbon surface species. TPD spectra of hydrogen formed during ethene adsorption on single-crystal surfaces available in literature show "two partially resolved subsidiary

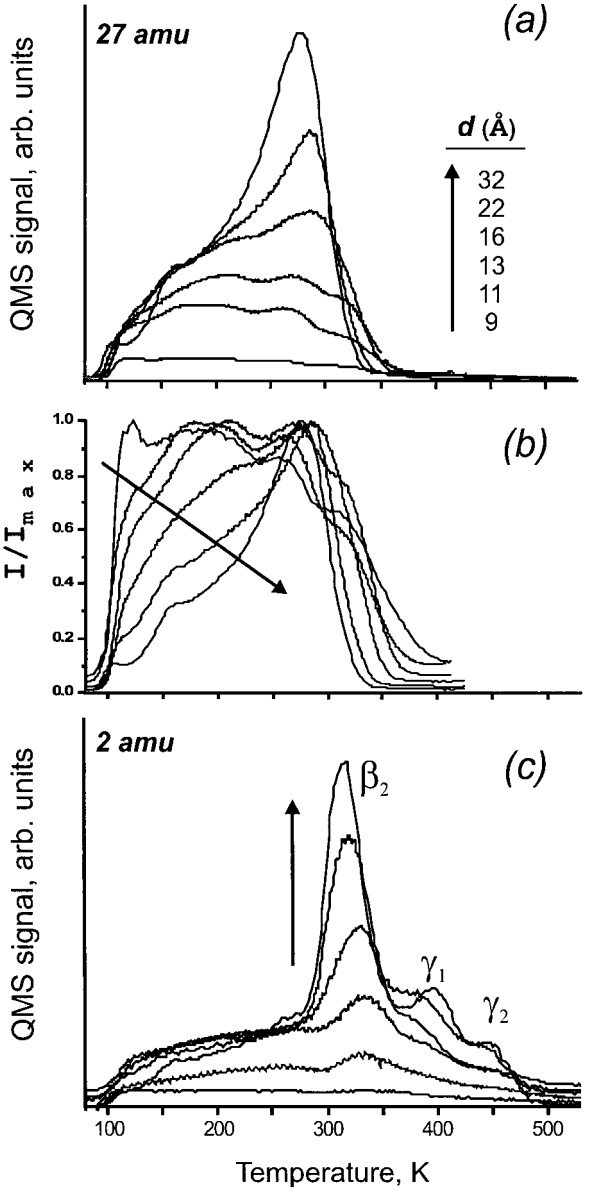

FIG. 3. (a) TPD spectra of ethene (27 amu) obtained for Pd particles of different size after exposure to 1 L of C_2H_4 at 90 K. (b) The same spectra but normalized with respect to the maximum intensity in each case in order to highlight the gradual changes as a function of particle size. (c) TPD spectra of hydrogen (2 amu) produced by ethene adsorption and recorded simultaneously with spectrum a.

features" at 410 and 470 K on Pd(111) (28), γ_1 and γ_2 peaks (at ca. 400 and 480 K) on Pd(100) (16), and a single γ peak centered at 480 K on Pd(110) (28) beyond the β_2 peaks in each case. However, the stable intermediates of ethene dehydrogenation, which have been suggested on the basis of HREELS data presented in these papers, depend on the surface structure. Therefore, on the supported small Pd particles exposing various crystallographic planes, it is difficult to assign precisely the steps of ethene dehydrogenation on the basis of TPD results only, at the present time.

Thus, the results presented in Fig. 3 clearly indicate that ethene adsorption is sensitive to particle size. This behavior may, in principle, be attributed to the changes in electronic structure and/or morphology of the particles as a function of size (30).

The electronic structure of the Pd deposits has previously been studied with XPS (6). By analyzing the binding energy of the Pd 4*d* state it has been concluded that the Fermi energy of the Pd aggregates moves upward in energy with increasing Pd coverage. This implies that the ability of the metal to donate electrons into the π*-orbital of ethene increases with increasing particle size. Therefore, a stronger $sp^2 \rightarrow sp^3$ rehybridization of the carbon atoms, i.e., a gradual transition from π- to di-σ-configuration, is expected as the particle size increases.

Depending on their size, on the other hand, metal particles can expose differently coordinated surface atoms and hence different adsorption sites. In order to illustrate this effect, Fig. 4 shows two pairs of TPD spectra obtained for the samples as prepared at 90 K and the samples flashed to 400 K in a vacuum prior to ethene adsorption at 90 K. The spectra clearly show that the fresh samples exhibit much more intense signals in the low-temperature region than the flashed ones. For the smaller particles, the preheating attenuates the integral intensity by a factor of 2. The latter effect can be obviously attributed to the higher number of adsorption sites on the rough, nonannealed Pd particles.

Based on IRAS and vibrational spectroscopy studies, it is concluded that rough metal surfaces, and particularly highly dispersed palladium, preferentially adsorb ethene via a π-complex at low temperature (7, 12, 13, 29). Therefore, we attribute the low temperature ($T < 230$ K) TPD signals to the desorption of π-bonded ethene.

With increasing particle size, the relative intensity of the low-temperature ethene TPD signal decreases and the peak near room temperature becomes dominant in the spectra (see Fig. 3a), therefore indicating that, on average, ethene adsorbs more strongly on the larger particles. This conclusion is supported by the gradual increase of the hydrogen γ peaks in the TPD spectra presented in Fig. 3c. The latter fact means that ethene dehydrogenation and hence carbon deposition preferentially occur on the large particles.

In fact, by monitoring with XPS the total amount of carbon-containing species formed by ethene adsorption, we have observed that about 30% of the initial carbon species remain on the ~40 Å particles while only about 10% remain on the ~8 Å particles on heating from 90 to 300 K (7, 27). In addition, our previous IRAS study (7) has revealed that ethylidyne species are detected only on the relatively large Pd particles of ca. 40 Å. Also, the formation of the ethylidyne species has been observed in the temperature interval of 250–350 K, i.e., in the region of the most intense peak in the TPD spectra of ethene from the large particles (Figs. 2 and 3). Since it is di-σ-bonded ethene that converts to ethylidyne (12, 13), we can assign the TPD signal near room temperature to the desorption of di-σ-bonded ethene.

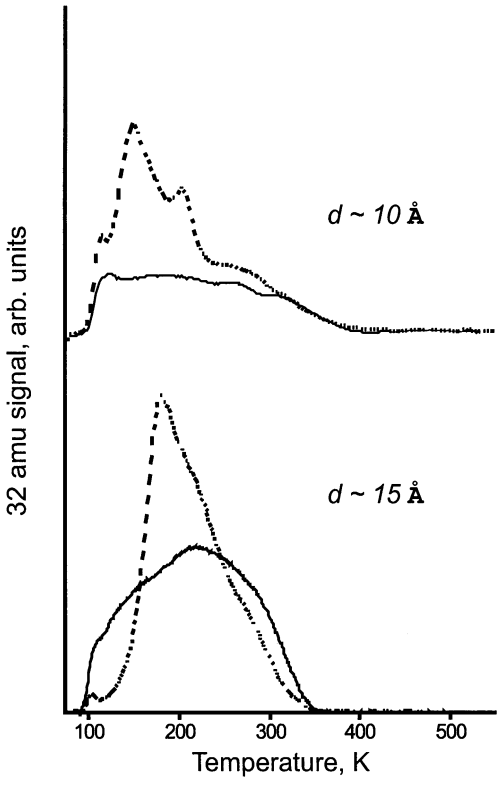

FIG. 4. TPD spectra demonstrating the effect of preheating on ethene adsorption (1 L of C_2D_4 at 90 K). Dashed lines correspond to samples prepared at 90 K, and solid lines correspond to samples prepared at 90 K and heated to 400 K in vacuum. The mean particle size is indicated.

Combining the results presented above, we can propose a general scheme for ethene thermal transformations on Pd particles, as depicted schematically in Fig. 5. On small Pd particles, ethene is mainly π-bonded at low temperatures and desorbs intact upon heating. On the larger Pd particles, however, a fraction of the ethene molecules is di-σ-bonded as previously shown by our IRAS study (7, 27). Again, weakly bonded ethene desorbs intact (its conversion to di-σ-species on heating cannot be excluded, however) while di-σ-ethene can either desorb near room temperature or dehydrogenate producing surface species, such as ethylidyne and atomic hydrogen. Dehydrogenation

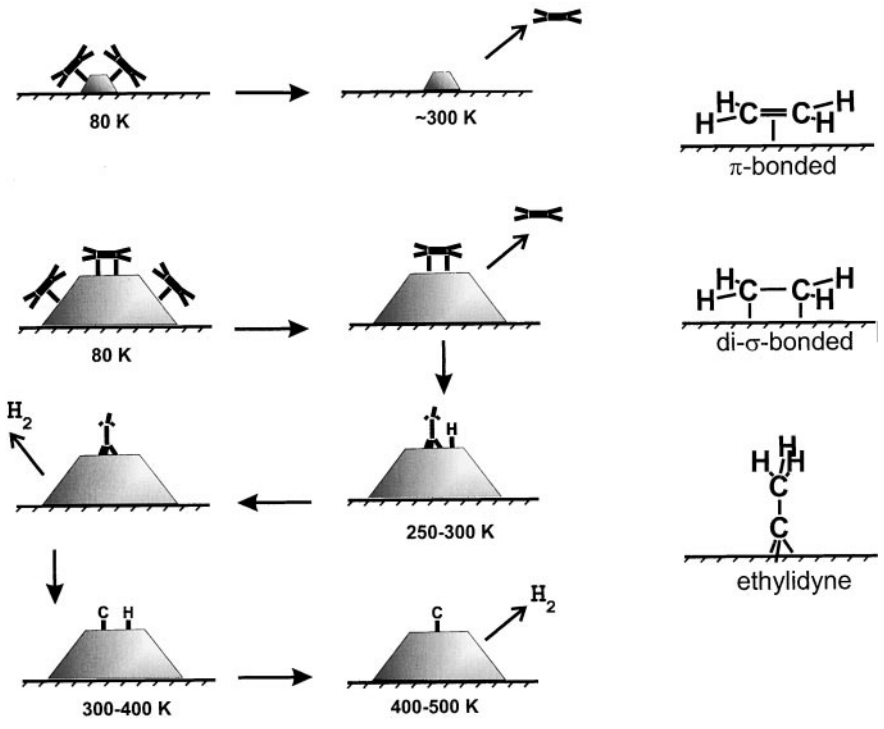

FIG. 5. A general scheme for the thermal transformations of ethene adsorbed on Pd particles.

proceeds further on heating until a hydrogen-deficient carbonaceous deposit and hydrogen are formed at elevated temperatures. Hydrogen atoms recombine and desorb as hydrogen molecules. Finally, the surface remains covered by carbon deposits at elevated temperatures.

Accordingly, particle size and roughness strongly influence the distribution of π- and di-σ-bonded ethene molecules. Due to the development of more extended facets on the large particles, which favor ethene di-σ-bonding, the reaction pathway shifts toward dehydrogenation and hence to the formation of carbon deposits on heating.

Hydrogen Adsorption

In the present study, we performed deuterium adsorption at 195 K. This temperature is close to the onset of the H_2 (D_2) TPD signals observed on Pd single-crystal surfaces at relatively low exposures when hydrogen dissolution into the bulk seems not to be essential (31–35). Note that lower adsorption temperatures have not been applied in order to avoid adsorption of H_2 from the vacuum background during sample cooling.

Figure 6a shows D_2 TPD spectra as a function of exposure for a particle size of ~34 Å in diameter. The saturation exposure corresponds to about 1.5 L. At least two adsorption states can be distinguished, centered at ca. 275 and 340 K and denoted as β_1 and β_2, respectively. The feature marked as β_0 appears at saturation exposure rather as a shoulder of the β_1 state and can be discriminated only by spectral deconvolution. For simplicity, we will use the term "β_1 state" bearing in mind that, in fact, it consists of two overlapping states.

There are no desorption states observed at T > 400 K, in contrast to the case of ethene adsorption (see Fig. 3c). Therefore, the γ states can definitely be attributed to the final steps of the complete ethene dehydrogenation process. On the other hand, no β_1 states are formed by ethene adsorption. This can be attributed to the fact that ethene dehydrogenation and hence formation of hydrogen adatoms occurs at temperatures higher than the desorption temperature of the β_1 states.

The temperature of the β_2 state decreases with increasing exposure, therefore indicating second-order desorption kinetics as shown Fig. 6a. This behavior is very similar to that observed on single-crystal surfaces (31–35). Indeed, for the case of relatively low H_2 exposures (below 2 L), TPD spectra have revealed the presence of a single desorption peak, centered at 310 K for Pd(111) (33), at 300 K for Pd(110) (32), and at 350 K for Pd(100) (31, 34), respectively, which follow second-order desorption kinetics due to recombination of the H ad-atoms.Therefore, it seems straightforward to assign the β_2 state to hydrogen atoms chemisorbed on the Pd particle surface.

Regarding the β_1 states, it is difficult to make a definitive assignment. According to Okuyama *et al.* (34), any state observed beyond the single peak at ~300 K on Pd(100) might indicate penetration of hydrogen atoms into subsurface regions which, as the authors have suggested, occurs at

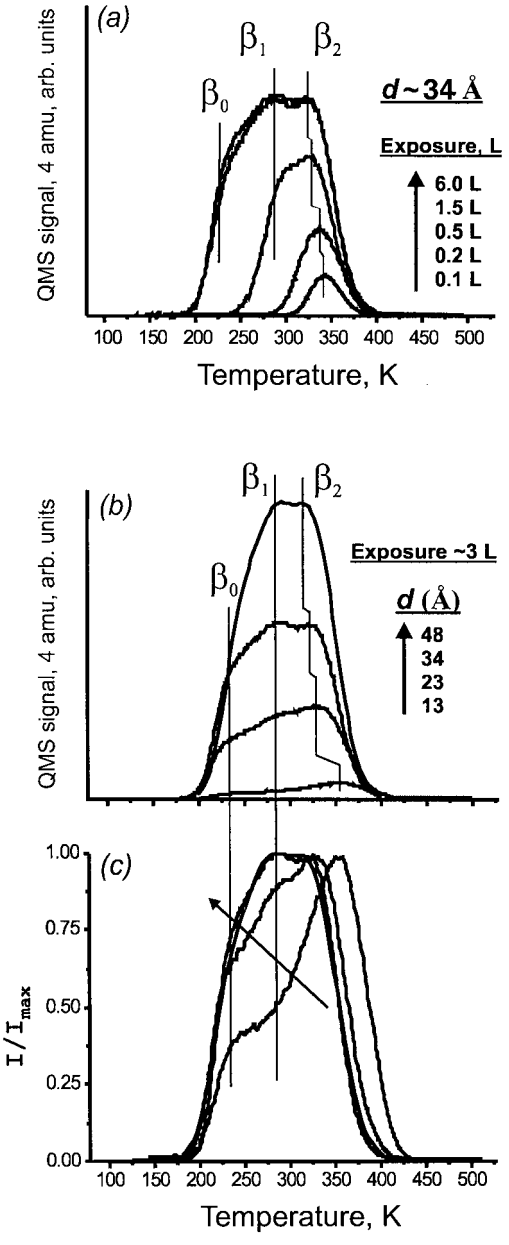

FIG. 6. TPD spectra of D_2 adsorbed on Pd particles at 195 K as a function of exposure (a) and of particle size (b, c). The spectra (c) are normalized with respect to the maximum intensity in each case in order to highlight the gradual changes in the spectra with increasing particle size.

defects on the Pd(100) surface. Similarly, Farias *et al.* (35) have assigned the β_1 state centered at ca. 280 K on Pd(331) to hydrogen residing in *sub*surface sites. On the Pd(210) surface, Muschiol *et al.* (20) have observed two states (β_2 and β_3 in their notation), which behave similarly to the β_1 and β_2 states in our study. Despite the more open surface structure, the authors have nevertheless assigned both states to chemisorption *on* the surface. Interestingly, only a single chemisorbed state has been resolved by TPD on Pd(111), although *surface* sites and *subsurface* sites between the first and second metal layers are occupied (33). This is probably due to a very small energy difference between the two states as calculated by Daw and Foiles (36).

It is considered that defect sites play an important role in hydrogen absorption [see, for example, Ref. 34]. Since the small particles are naturally defective, we tentatively attribute the β_1 states as corresponding to *subsurface* hydrogen.

Figure 6b shows a family of TPD spectra of D_2 desorbing from Pd particles of different sizes at saturation exposure. The temperature of the β_2 state shifts to lower temperatures with increasing particle size. This indicates that *surface* hydrogen chemisorbs more weakly on the larger particles. This is in line with a calorimetric study 64 Chou and Vannice (37), which showed that the integral heat of adsorption of hydrogen on highly dispersed Pd increased sharply when the size dropped below 3 nm.

Formation of the β_1 states is suppressed on the smallest particles, as shown in the normalized TPD spectra presented in Fig. 6c. This can result from the decreasing number of subsurface sites available, or from the influence of the alumina support underneath, or both. Nevertheless, the desorption temperatures of β_1 (and β_0) states seem not to be influenced by the particle size.

Ethene and Hydrogen Co-adsorption

Figure 7 shows TPD spectra obtained after ethene adsorption on the clean (spectra a) and the D_2 presaturated

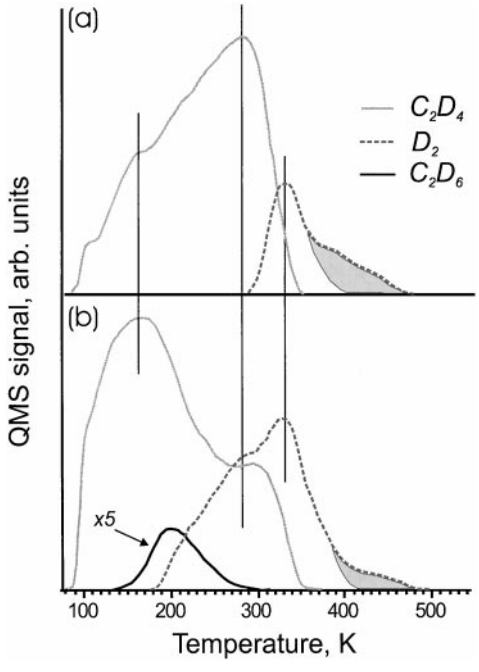

FIG. 7. TPD spectra of D_2 (4 amu), C_2D_4 (32 amu), and C_2D_6 (36 amu) obtained under the following adsorption conditions: (a) 1 L of C_2D_4 at 90 K; (b) 3 L of D_2 at 195 K followed by 1 L of C_2D_4 at 90 K. The mean Pd particle size is about 20 Å. Note that the contributions to 4 amu and 32 amu signals resulting from the cracking pattern of ethene and ethane have been subtracted.

(spectra b) Pd particles of identical size. We recorded the signals of masses corresponding to D_2, C_2D_4, and C_2D_6. (In the following spectra the contributions of the ethene and ethane cracking patterns to the 4 and 32 amu signals have been subtracted for clarity.) Comparing these spectra, first, we observe the formation of ethane, desorbing at ~200 K as the product of ethene hydrogenation. Second, the amount of ethene desorbing at temperatures below 200 K is significantly increased, while the intensity of the state at about 280 K is reduced by a factor of 2. In addition, the intensity of the D_2 γ states, corresponding to ethene decomposition, are decreased under co-adsorption as indicated by the gray shading. Note that both states, the ethene signal at ~280 K as well as the γ states of D_2, have been attributed above to the desorption and dehydrogenation of di-σ-bonded ethene, respectively. Therefore, the data clearly indicate that it is the formation of di-σ-ethene that is inhibited by D adatoms. This can be understood by assuming that the surface D atoms, residing presumably in the hollow sites, sterically hinder the di-σ-bonding. Meanwhile, ethene can readily adsorb on the D-covered surface via a π-bond on on-top sites. Therefore, hydrogen preadsorption leads to a redistribution of π- and di-σ-bonded ethene, thus favoring a weakly bonded π-state.

In the reverse experiments, when the Pd particles were ethene precovered before exposure to D_2, the spectra were found to be identical to those when there was no D_2 exposure at all. This clearly manifests a site-blocking effect of ethene on hydrogen adsorption. Such an effect can be readily explained by the fact that adsorption of molecular hydrogen on metals exhibits an "ensemble effect" and that hydrogen dissociation occurs on on-top sites [see review in Ref. (17)], which are occupied by ethene.

In the absence of preadsorbed hydrogen, a very small amount of ethane desorbing at ca. 280 K was detected only for particles larger than 30 Å. This process, called self-hydrogenation, involves the reaction of ethene with hydrogen adatoms produced by dehydrogenation of other ethene molecules. Certainly, such a reaction occurs only on the relatively large particles due to an increasing probability of ethene dehydrogenation (see Fig. 5). Nevertheless, the amount of ethane produced by self-hydrogenation is negligibly small as compared to that detected in co-adsorption experiments. Moreover, the desorption temperature of ethane formed under co-adsorption conditions is about 80 K lower than that in a self-hydrogenation reaction (200 K vs 280 K). Such a behavior (a temperature shift and an enhanced ethane production) has also been found on hydrogen precovered Pt(111) (38) and Pd(110) (29) surfaces. Therefore, it appears that a general mechanism of ethene interaction with hydrogen on metal surfaces is valid on both single crystals and small metal particles.

In the co-adsorption experiments resulting in ethane formation, we presaturated the Pd particles with D_2 at 195 K

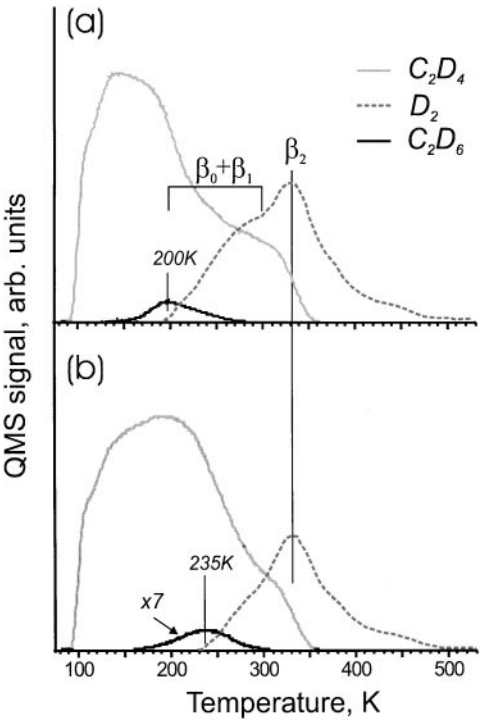

FIG. 8. TPD spectra of D_2 (4 amu), C_2D_4 (32 amu), and C_2D_6 (36 amu) after adsorption of 3 L of D_2 at 195 K (a) and 300 K (b) followed by exposure to 1 L of C_2D_4 at 90 K. The positions of the adsorption states as observed after adsorption of D_2 on the clean Pd particles are indicated. The mean particle size is about 20 Å.

in order to compare the TPD spectra obtained under adsorption and co-adsorption conditions. Therefore, both β_1 and β_2 states have been filled prior to ethene adsorption. In order to determine which state participates in the hydrogenation reaction, we have performed experiments by pre-adsorbing D_2 at 195 and 300 K. The latter temperature is significantly higher than the desorption temperature of the β_1 states (220–270 K) and therefore its formation should be suppressed.

Unfortunately, formation of the β_1 states cannot be completely avoided, as shown in Fig. 8b, probably due to readsorption of D_2 from the vacuum background during the subsequent cooling of the sample from 300 to 90 K for ethene adsorption. Nevertheless, the amount of ethane produced under these conditions, i.e., in the deficiency of D atoms in the β_1 state, is about 7 times lower compared to the case where both states are populated [cf. (a) and (b) in Fig. 8]. Furthermore, the ethane desorption temperature is shifted from 200 to 235 K, apparently following the onset of D_2 desorption. Therefore, we can conclude that ethene reacts with the most weakly bonded hydrogen present on the surface. Since the β_2 state corresponds to temperatures at which only di-σ-bonded ethene and ethylidyne species exist on the surface, the strongly bonded H (D) adatoms are probably involved in the

reaction only in a manner similar to a self-hydrogenation process.

Thus, the data show that the formation of ethane depends on the presence of weakly adsorbed hydrogen which reacts with π-bonded ethene before the latter desorbs intact. Therefore, there must be an overlap of desorption states of π-bonded ethene and β_1 hydrogen in the TPD spectra for the reaction to occur.

Influence of Particle Size on Ethene and Hydrogen Reaction

It is interesting to compare the TPD results obtained for samples of different particle sizes. For this purpose, we have carried out experiments for identical preparations varying only the particle size. The samples were prepared by Pd deposition at 90 K and subsequent heating to 400 K in vacuum. The samples were then exposed to 3 L of D_2 at 195 K followed by adsorption of 1 L of C_2D_4 at 90 K.

Figure 9 shows the plot of ethane production per Pd unit surface area as a function of particle size. This plot clearly demonstrates that the hydrogenation activity under the coadsorption conditions studied is almost independent of the Pd particle size in the 1–3 nm range.

Such a behavior can be understood if one takes into account the general observations discussed in detail in the previous sections. Let us begin with the fact that the hydrogenation reaction occurs between the π-bonded ethene and hydrogen in the most weakly bound (β_1) state. The formation of the latter species strongly depends on the adsorption temperature, as judged by the onset of the D_2 desorption in Figs. 6c and 8. Of course, the relative population of β_1 with respect to the β_2 state depends on the particle size, as shown in Fig. 6c, and therefore one could expect a particle size dependence if all β_1 hydrogen atoms were consumed in the reaction. However, the fraction of the preadsorbed hydrogen that has reacted with ethene to form ethane is too low: less than 20% of the overall amount of ethene was hydrogenated in the present set of experiments. Also, preadsorbed hydrogen strongly inhibits the formation of di-σ-bonded ethene and results in preferential formation of the π-bonded ethene for all particle sizes studied, thus neutralizing the overall particle size influence. Therefore, all the above reasons favor a rather small particle size dependence of ethene hydrogenation on Pd particles.

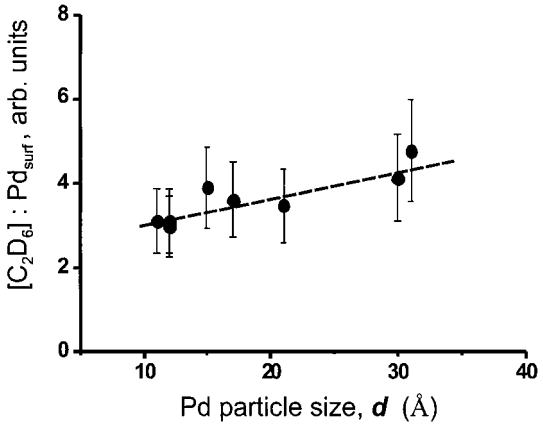

FIG. 9. Integral TPD signal of ethane per Pd unit surface area as a function of particle size measured after identical co-adsorption conditions: 3 L of D_2 at 195 K followed by 1 L of C_2D_4 at 90 K.

It should also be mentioned that the absence of a particle size effect on the reaction may indicate that the rate-determining step for ethene hydrogenation is the addition of a hydrogen atom (that is, hydrogen in β_1 states) to either a C_2H_4 or a C_2H_5 surface species.

The size independence for ethene hydrogenation obtained in the present work agrees well with the general opinion that this reaction is structure insensitive (8). However, the data presented by Masson *et al.* (10) show about 3 times higher turnover frequency in ethene hydrogenation on Pt particles with a size about 0.6 nm. Those measurements were performed at 250°C under atmospheric pressure on Pt vapor-deposited on SiO_2 and Al_2O_3, thus indicating a notable size effect for very small metal clusters. However, for particles in the 1–3 nm range, both Masson's and present studies show a particle size independence. Please note that in the study by Masson *et al.* the reaction conditions are very different from the present ones and we have to see how these conditions affect the particles of smallest size. Nevertheless, it seems that our system represents a suitable model system for studying the mechanism of the reaction, even under UHV conditions.

In the experiments presented above we have considered particle size while the particle shape was not controlled. To control the shape is rather difficult for the samples studied in the present work (low-temperature Pd deposition and thermal "flash" to 400 K). In contrast, the particles are well-shaped when deposited at room temperature, exhibiting (111) and (100) facets as resolved by STM [see Fig. 1d, and Ref. (23)]. We have performed a few co-adsorption experiments with Pd deposits prepared at room temperature. Under identical adsorption conditions, the ethane production turned out to be lower by a factor of 5 for the same Pd surface area. This strongly suggests that ethene hydrogenation depends on the particle *morphology*. Particles with well-ordered (111) facets appear to be less active. Further work is in progress to explore this important matter further.

SUMMARY

The TPD results presented in this paper show that both ethene and hydrogen adsorption on Pd particles supported on a thin alumina film are particle size sensitive. Ethene adsorption strength increases gradually with increasing size.

This has been attributed to a redistribution of π- and di-σ-bonded ethene, the latter preferentially adsorbing on the large particles, thus shifting the overall desorption temperature to higher values. A general scheme for ethene thermal transformations on Pd particles has been suggested using the complementary information from TPD, IRAS, and XPS studies on single-crystal surfaces and literature data on highly dispersed catalysts.

Deuterium adsorption at 195 K on Pd particles results in at least two states with desorption temperatures of ca. 270 and 330 K. The latter state exhibits second-order desorption kinetics and is assigned to hydrogen located on the surface. The overlapping low-temperature states are assigned to subsurface hydrogen. Our data show that surface hydrogen adsorbs more strongly on the smaller particles.

Co-adsorption studies of ethene and hydrogen show that preadsorbed ethene inhibits hydrogen adsorption. In turn, hydrogen adatoms shift the distribution of π- and di-σ-ethene states toward a higher population of weakly π-bonded ethene. π-bonded ethene and hydrogen in the weakly bound (subsurface) states are involved in the hydrogenation reaction, as revealed by the TPD results.

The relationship between ethane production and Pd surface area shows that, under the conditions studied, the hydrogenation activity is independent of the particle size in the 1–3 nm range. However, preliminary data indicate that the reactivity depends on the particle morphology. Particles with well-ordered (111) facets seem to be less active.

The TPD results obtained in this work are in good agreement with the proposed scheme of ethene hydrogenation, suggesting that π-bonded ethene is the reactive species (39, 40).

ACKNOWLEDGMENTS

The authors gratefully acknowledge M. Frank for providing XPS and IRAS data, J. Hemminger for fruitful discussions, and M. Naschitzki for technical assistance. This work is supported by ICI plc through the Strategic Research Fund. D.L. thanks ICI for the award of an ICI Lectureship in Heterogeneous Catalysis.

REFERENCES

1. Gunter, P. L. J., Niemantsverdriet, J. W. H., Ribeiro F. H., and Somorjai, G. A., *Catal. Rev.- Sci. Eng.* **39**, 77 (1997).
2. Henry, C. R., *Surf. Sci. Rep*. **31**, 231 (1998).
3. Goodman, D. W., *Surf. Rev. Lett.* **2**, 9 (1995).
4. Campbell, C. T., *Surf. Sci. Rep*. **27**, 1 (1997).
5. Freund, H.-J., *Angew. Chem., Int. Ed. Engl.* **36**, 452 (1997).
6. Bäumer, M., and Freund, H.-J., *Prog. Surf. Sci.* **61**, 127 (1999).
7. Frank, M., and Bäumer, M., *Phys. Chem. Chem. Phys.* **2**, 3723 (2000).
8. Somorjai, G. A., "Introduction to Surface Chemistry and Catalysis." Wiley, New York, 1994.
9. Hub, S., Hilaire, L., and Touroude, R., *Appl. Catal*. **36**, 307 (1988).
10. Masson, A., Bellamy, B., Hadj Romdhane, Y., Che, M., Roulet, H., and Dufour, G., *Surf. Sci*. **173**, 479 (1986).
11. Otero Schipper, P. H., Wachter, W. A., Butt, J. B., Burwell, R. L., and Cohen, J. B., *J. Catal*. **50**, 494 (1977).
12. Sheppard, N., and De La Cruz, C., *Adv. Catal*. **41**, 1 (1996).
13. Sheppard, N., and De La Cruz, C., *Adv. Catal*. **42**, 181 (1998).
14. Gates, J. A., and Kesmodel, L. L., *Surf. Sci*. **124**, 68 (1983).
15. Nishijima, M., Yoshinobu, J., Sekitani, and Onchi, M., *J. Chem. Phys*. **90**, 5114 (1989).
16. Stuve, E. M., Madix, R. J., and Brundle, C. R., *Surf. Sci*. **152/153**, 532 (1985).
17. Christmann, K., *in* "Hydrogen Effects in Catalysis" (Z. Paal and P. G. Menon, Eds.), p. 3. Dekker, New York, 1988.
18. Palczewska, W., *in* "Hydrogen Effects in Catalysis" (Z. Paal and P. Menon, Eds.), p. 373. Dekker, New York, 1988.
19. Christmann, K., *Surf. Sci. Rep*. **9**, 1 (1988).
20. Muschiol, U., Schmidt, P. K., and Christmann, K., *Surf. Sci*. **395**, 182 (1998).
21. Jaeger, R. M., Kuhlenbeck, H., Freund, H.-J., Wuttig, M., Hoffmann, W., Franchy, R., and Ibach, H., *Surf. Sci*. **259**, 235 (1991).
22. Bäumer, M., Frank, M., Heemeier, M., Kühnemuth, R., Stempel, S., and Freund, H.-J., *Surf. Sci*. **454/456**, 957 (2000).
23. Hansen, K. H., Worren, T., Stempel, S., Lægsgaard, E., Bäumer, M., Freund, H.-J., Besenbacher, F., and Stensgaard, I., *Phys. Rev. Lett*. **83**, 4120 (1999).
24. Stempel, S., Bäumer, M., and Freund, H.-J., *Surf. Sci*. **402/404**, 424 (1998).
25. Frank, M., Kühnemuth, R., Bäumer, M., and Freund, H.-J., *Surf. Sci*. **427/428**, 288 (1999).
26. Jaeger, R. M., Libuda, J., Bäumer, M., Homann, K., Kuhlenbeck, H., and Freund, H.-J., *J. Electron. Spectrosc. Relat. Phenom*. **64/65**, 217 (1993).
27. Frank, M., Bäumer, M., Kühnemuth, R., and Freund, H.-J., *J. Vac. Sci. Technol*., in press.
28. Tysoe, W. T., Nyberg, G. L., and Lambert, R. M., *J. Phys. Chem*. **88**, 1960 (1984).
29. Sekitani, T., Takaoka, T., Fujisawa, M., and Nishijima, M., *J. Phys. Chem*. **96**, 8462 (1992).
30. Che, M., and Bennett, C. O., *Adv. Catal*. **20**, 153 (1989).
31. Behm, R. J., Christmann, K., and Ertl, G., *Surf. Sci.* **99**, 320 (1980).
32. Behm, R. J., Penka, V., Cattania, M.-G., Christmann, K., and Ertl, G., *J. Chem. Phys*. **78**, 12 (1983).
33. Gdowski, G. E., Felter, T. E., and Stulen, R. H., *Surf. Sci*. **181**, L147 (1987).
34. Okuyama, H., Siga, W., Takagi, N., Nishijima, M., and Aruga, T., *Surf. Sci*. **401**, 344 (1998).
35. Farias, D., Patting, M., and Rieder, K. H., *Phys. Stat. Sol*. **159**, 255 (1997).
36. Daw, M. S., and Foiles, S. M., *Phys. Rev. B* **35**, 2128 (1987).
37. Chou, P., and Vannice, A. M., *J. Catal*. **104**, 1 (1987).
38. Godbey, D., Zaera, F., Yeates, R., and Somorjai, G. A., *Surf. Sci*. **167**, 150 (1986).
39. Beebe, T. P., and Yates, J. T., Jr., *J. Am. Chem. Soc*. **108**, 663 (1986).
40. Cremer, P. S., and Somorjai, G. A., *J. Chem. Soc., Faraday Trans*. **91**, 3671 (1995).